Intelligent Ultrasonic Flow Measurement Using Linear Array Transducer With Recurrent Neural Networks

THI HUONG LY NGUYEN AND SUHYUN PARK[ID]

School of Electrical and Electronics Engineering, Chung-Ang University, Seoul 06974, South Korea

Corresponding author: Suhyun Park (suhyun@cau.ac.kr)

ABSTRACT To realize high-quality transit-time ultrasonic flow measurements, accurate and precise estimates of the transit-time difference are essential. In this study, we propose deep learning-based neural network (NN) models to measure the transit-time difference in an ultrasonic flowmeter using a linear array transducer. Three approaches to compute the transit-time difference are presented: the cross-correlation with phase zero-crossing (XCorr), fully connected NN, and recurrent neural network (RNN) with long short-term memory (LSTM). The training data for the NN were generated by simulating target time differences by utilizing the experimental data acquired in the pipe system. To evaluate the performance of the proposed methods, linear regression, the Bland–Altman plot, and the root mean squared error (RMSE) were analyzed using testing data from the experiment. The results of this study show that the RNN-based approach yielded improved performance with an accuracy of up to 94% and a 33.48% reduction in the RMSE, compared to the XCorr method. In addition to the time difference estimation, our proposed RNN-based model can replace the entire flow rate estimation process, including interpolation, velocity correction, and zero-flow calibration. This study demonstrates the feasibility of an intelligent ultrasonic flowmeter employing the RNN-based model with potential in industrial applications.

INDEX TERMS Deep learning, recurrent neural network, transit-time estimation, ultrasonic flowmeter.

I. INTRODUCTION

The ultrasonic flowmeter has been employed for liquid flow rate measurements in industrial and medical fields, such as in pump stations to ensure the energy efficiency of building management systems and in wrist sensors for blood flow monitoring, respectively, owing to its high sensitivity to flow changes [1]–[5]. The transit-time method has widespread applicability for the non-invasive measurement of the flow of particle-free fluids through pipes [6]–[8]. The transit-time ultrasonic flowmeter obtains the fluid flow rate from the transit-time difference of ultrasonic signals between the downstream and upstream of the flow. Ultrasonic signals originate from reflections arising due to the impedance mismatch between the pipe walls and the fluid. Various factors can degrade the performance of the transit-

time ultrasonic flowmeter, such as a misalignment of ultrasonic sensors, irregular pipe surface conditions, and errors in the transit-time difference estimation. The accuracy of the ultrasound flowmeter can be improved by reducing errors in the transit-time estimation.

Our previous study [9] demonstrated the feasibility of a transit-time ultrasonic flowmeter employing an ultrasonic linear array transducer in a designed pipe system. The transit-time difference was estimated by the cross-correlation with phase zero-crossing (XCorr) method. The accuracy of the flowmeter was enhanced by exploiting the properties of ultrasonic array sensors. However, the ultrasonic flowmeter requires further improvement in the transit-time difference estimation, especially when the data acquisition system suffers from a sampling rate limitation.

Previous studies [10]–[17] employed several approaches to achieve higher accuracies in the ultrasonic flowmeter. One study reported that computing the phase difference using a

The associate editor coordinating the review of this manuscript and approving it for publication was Filbert Juwono[ID].

T. H. L. Nguyen, S. Park: Intelligent Ultrasonic Flow Measurement Using Linear Array Transducer With Recurrent Neural Networks

IEEE Access

least-squared-sine-fitting algorithm could reduce the measurement error of the transit-time [10]. Another group studied an auto-adaptive impulse response function estimation technique to avoid false peaks in the correlation method [11]. They also reported that a higher sampling rate is capable of improving the flow measurement performance. In addition to the signal processing approaches, a study employed pattern recognition algorithms, which classified the flow velocity profile in a pipe, to reduce the uncertainty in ultrasonic flow measurements [12]. In recent years, deep learning approaches based on neural networks (NNs) have undergone rapid developments to solve prediction and classification problems in various fields [18]–[21]. Furthermore, these approaches are useful for signal and image processing, pattern recognition, and forecasting. Concepts of the NN were likewise applied to improve ultrasonic flowmeters in previous studies [14]–[17]. By employing a NN model consisting of a single-layer NN and a two-layer perceptron network, a previous study demonstrated the interpolation of flow velocity profiles and weight calculation for different ultrasound paths [14]. Their results indicate reduced errors in the ultrasonic flowmeter measurements. However, the flowmeter performance was limited due to the adoption of a simple NN model. Another study utilized a three-layer NN (including one hidden layer) to acquire the weight factor for a multi-path ultrasonic flowmeter, in order to reduce errors in flow distortion [15]. The accuracy of the multi-path ultrasonic flowmeter was further improved by using the generalized inverse of matrix [13], the extreme learning machine method [16], and NNs based on the genetic algorithm [17].

Although previous studies have demonstrated the potential of NNs in improving the performance of ultrasonic flow measurements, a majority of these studies were conducted during the early stages of the development of NNs. Thus, the applicability of these studies is limited, as only part of the problem of ultrasonic flowmeters was solved. This study proposes an intelligent ultrasonic flowmeter. To the best of our knowledge, this is the first implementation of the complete process of flow rate estimation using a single deep NN model. First, we introduce the complete flow rate estimation process of the ultrasonic flowmeter. Thereafter, to enhance the accuracy of flow estimation, an intelligent ultrasound flowmeter was designed utilizing two NN models, namely the fully connected NN and the recurrent neural network (RNN)-based model with long short-term memory (LSTM) [18], [22]–[28]. The NN models were trained using simulated and experimental ultrasonic data. Finally, the performance of the proposed intelligent ultrasonic flowmeter was evaluated using the experimental data acquired from the pipe system for various flow rates.

II. MATERIALS AND METHODS
A. DATA ACQUISITION
The experimental setup of the pipe (SUS304) system with the water flow is presented in Fig. 1. The outer diameter, inner diameter, and thickness of the pipes were 34, 27.6,
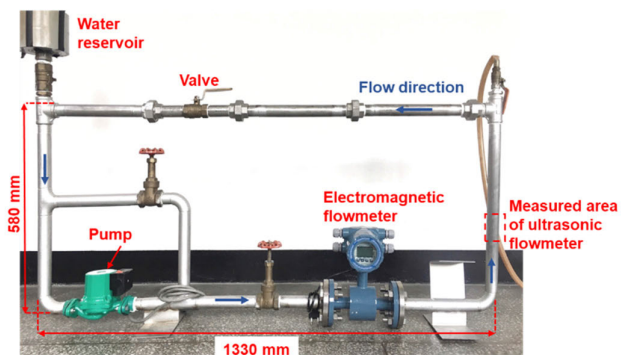

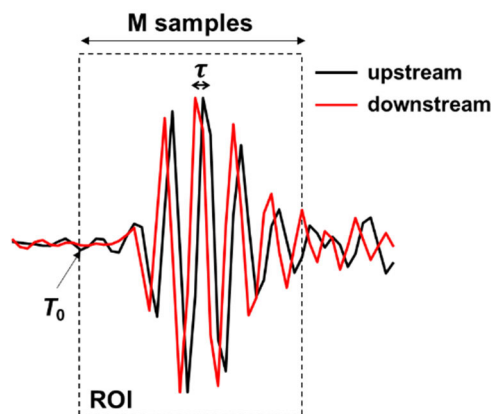**FIGURE 1.** Experimental setup for liquid flow measurements.

FIGURE 2. RF signals received from upstream and downstream of flow.

and 3.2 mm, respectively. Ultrasonic radio frequency (RF) data from the single path were collected at various flow rates between 0 L/min and 50 L/min (approximately at 0, 7, 10, 15, 20, 25, 35, and 50 L/min). The reference flow rates were recorded in real-time through the pipe system by using an electromagnetic flowmeter (FMAG550G, Flos Korea Inc., Seoul, Korea). Ultrasonic plane waves for both the upstream and downstream of the liquid were transmitted and received via the ultrasound imaging system (Vantage 32LE$^{\text{TM}}$, Verasonics Inc., Kirkland, USA) and the linear array transducer (ATL L7-4, ATL Ultrasound Inc., Bothell, USA). The transmission frequency of the transducer was 5.2 MHz, and the data acquisition sampling rate was 20.8 MHz. Based on the angles of the transmitted plane waves, the received ultrasound RF signals of the matching transmitter and receiver elements for the single path were selected for the flow rate estimation (Table 1 in [9]). The transmission angle used in this study was in the range of 19.88°–20.38°.

Fig. 2 presents an example of the received ultrasound RF signals from the upstream and downstream of the fluid. The signals in the region-of-interest (ROI) within the box were used for transit-time estimation. The start position of the ROI (T_0) was calculated based on the traveling time of the ultrasound signal in the pipe. In this study, the length M of
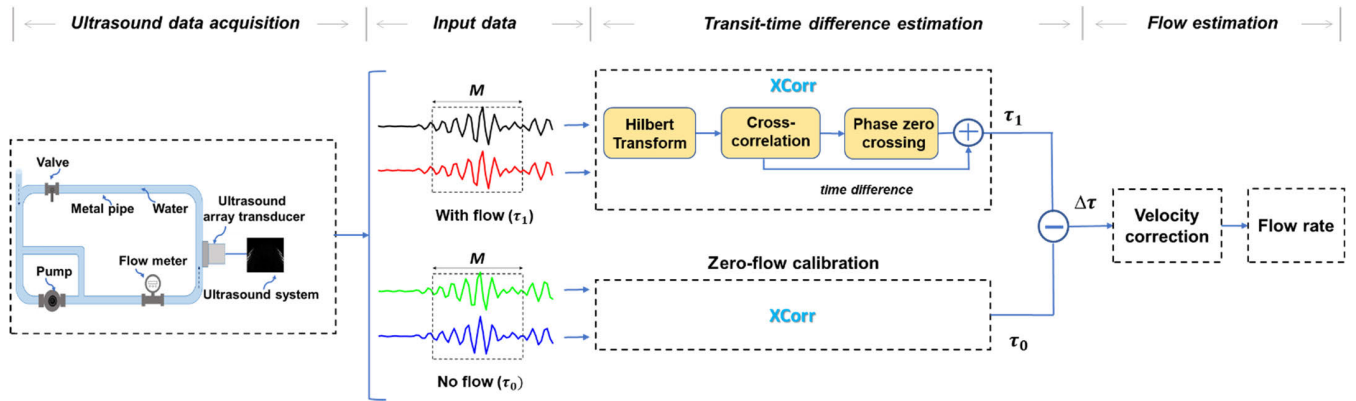
FIGURE 3. Block diagram of flow rate estimation using the XCorr method.

the ROI was fixed to 33 samples, which corresponds to a duration of 1.5841 μs. A total of 106 ultrasound examples acquired from the experiment were utilized to determine the flowrates.

B. FLOW RATE ESTIMATION

For a pipe with diameter D, the upstream transit-time t_{up} and downstream transit-time t_{down} are described as

$$t_{up} = \frac{L}{c - V sin(\theta)} \quad (1)$$

$$t_{down} = \frac{L}{c + V sin(\theta)}, \quad (2)$$

respectively, where L is the ultrasonic path length, c is the speed of sound in the fluid, V is the average flow velocity, and θ is the incident angle of the ultrasonic wave. As the fluid flow velocity is significantly lower than the speed of sound ($V \ll c$), the flow rate (Q) can be calculated as follows:

$$Q = K \frac{\pi D^2 c^2}{8L sin\theta} \left(t_{up} - t_{down} \right) = K \frac{\pi D^2 c^2}{8L sin\theta} \tau, \quad (3)$$

where K is the correction factor denoting the ratio of the average velocity in the pipe and the velocity measured along the ultrasonic beam, and τ is the transit-time difference in the single path [6]–[8].

Fig. 3 illustrates a block diagram of the flow rate estimation process for a fluid flowing in the pipe system. First, the ultrasonic RF data from the upstream and downstream (Fig. 2) were acquired at varying flow rates and also when there was no flow in the pipe. The data acquired in the no-flow condition was used for zero-flow calibration, which compensated the time-shift offsets arising due to the physical conditions of the pipe and sensors [9]. In our previous study, the transit-time difference estimation was performed using the XCorr method [9]. In the transit-time estimation process, the acquired RF data were transformed into analytic signals via the Hilbert transform. Thereafter, the time difference in the sampling interval was estimated from the cross-correlation peak. After cross-correlation, the phases of the cross-correlation were linearly interpolated by a factor

of 100 near the peak. To achieve the sub-sample level time difference, the time required to cross the zero phase was determined [29], [30]. Hence, the transit-time differences (τ_1 with flow and τ_0 without flow) were acquired by the summation of the time differences obtained via the XCorr method. After the zero-flow calibration ($\Delta\tau = \tau_1 - \tau_0$), velocity correction was applied to the estimated transit-time difference ($\Delta\tau$). In this study, the velocity correction factor K was 0.93–0.94, depending on the flow rate [9], [31]. Finally, the fluid flow rate of the pipe system was determined using (3).

C. NN BASED APPROACHES

1) DATA GENERATION

The training data for the NN were generated using 50 experimental RF signals acquired from the pipe system. Although the transit-time difference (i.e., τ in (3)) exhibits a continuous nature of the flow, the experimental data cannot be collected under all possible transit-time differences. To overcome this limitation, training data with varying transit-time differences were generated by randomly shifting the RF signals acquired during the experiment. Prior to data generation, the amplitude of the experimental signals was normalized in the range of −1 to +1 to avoid signal scale variation. By denoting one of the acquired RF signals from the experiment as $s_1(t)$, where t is the time, the signals from the upstream ($u_1(t)$) and downstream ($d_1(t)$) of the flow were generated as

$$u_1(t) = s_1(t) + n_1(t) \quad (4)$$

$$d_1(t) = s_1(t - \tau_1) + n_2(t), \quad (5)$$

respectively, where τ_1 is the transit-time difference between the RF signals from the upstream and downstream of the flow, and n_1 and n_2 are the additive Gaussian random noises for data augmentation using a randomized standard deviation within the range of 0 to 0.1. One thousand transit-time differences (τ_1) were randomly generated between −1.5 to 1.5 samples (i.e., −0.072 μs to 0.072 μs) using experimental data. Thus, a total of 50,000 training data sets, with $M \times 2$ ultrasonic RF data sample points per data set, were generated for the fully connected NN model.
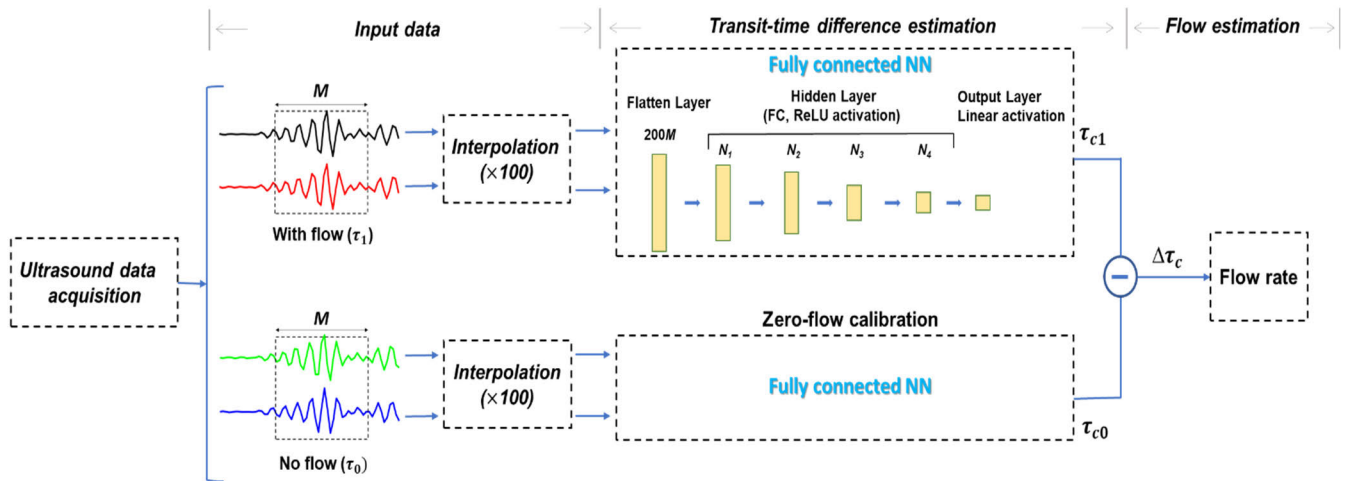
T. H. L. Nguyen, S. Park: Intelligent Ultrasonic Flow Measurement Using Linear Array Transducer With Recurrent Neural Networks

IEEE *Access*

FIGURE 4. Flow estimation block diagram in fully connected NN.

For the fully connected NN, the same training data sets were utilized to train the network for both flow and no-flow cases. However, for the RNN-based model, the training data sets were generated separately for the flow and no-flow cases. The training data including flow from the upstream and downstream ($u_1(t)$ and $d_1(t)$) were generated using (4) and (5), respectively. Further, the training data at the no-flow condition ($u_0(t)$ and $d_0(t)$) were generated using the acquired RF signal $s_0(t)$, as follows:

$$u_0(t) = s_0(t) + n_3(t) \qquad (6)$$
$$d_0(t) = s_0(t - \tau_0) + n_4(t), \qquad (7)$$

where n_3 and n_4 are the additive Gaussian random noises for data augmentation using a randomly selected standard deviation between 0 to 0.1. From 50 experimental RF signals, 100 combinations of flow and no-flow data were generated. For each combination, 1000 transit-time differences after zero-flow calibration and velocity correction (i.e., $\Delta\tau_c$) were randomly generated between 0 to 0.8170 samples, which correspond to flow rates from 0 L/min to 70 L/min. Therefore, a total of 100,000 training data sets, with $M \times 4$ ultrasonic RF data sample points per data set, were generated for the RNN-based model.

To estimate the generalization error during training, validation data sets were also generated using the same method as the training data sets. A total of 1000 validation data sets were generated from the experimental data. The validation data were used for evaluating the fully connected NN and the RNN-based models during the training of the NNs. Finally, the RF ultrasound data acquired from the experiment in the pipe system were used as the testing data. The experimental ultrasound examples were randomly split into training and testing data. The testing data comprised 56 experimental examples after excluding the 50 examples that were used for the generation of training and validation data. The amplitudes of the testing data were normalized in the range from −1 to 1.

2) FULLY CONNECTED NN-BASED APPROACH

The flow rate estimation process using the fully connected NN model is presented in Fig. 4. For the transit-time difference estimation, the signal processing blocks (i.e., Hilbert transform, cross-correlation, and phase zero-crossing) were replaced by the fully connected NN block. The training data (u_1 and d_1; $M \times 2$ array) were interpolated by a factor of 100. Subsequently, the interpolated data were fed into the flatten layer to reshape the data to one dimension for the fully connected layer. The size of the data after the flatten layer was 200M (i.e., 6600 samples). The flatten layer was followed by four hidden fully connected layers with a different number of neurons. The dimensionalities N_1, N_2, N_3, and N_4 of the hidden layers were 1300, 660, 330, and 165, respectively. The output of the two fully connected NN blocks comprised the transit-time differences τ_{c1} and τ_{c0}. Similar to our previous method, shown in Fig. 3, zero-flow calibration was applied to obtain the time difference $\Delta\tau_c$. Velocity correction was applied to the target output for training the fully connected NN. Thus, the flow rate was calculated from the time difference $\Delta\tau_c$ without the velocity correction process. The activation in the fully connected layer is computed by the following formula:

$$Y = f\left(W^T X + b\right), \qquad (8)$$

where X is the input vector, Y is the output vector, W is the weight matrix between the input and output, b is the bias vector, and f is the activation function. In our model, four hidden layers were activated by the rectified linear unit (ReLU) function. The activation of the output layer is the linear activation function because the output of the fully connected NN model is the time difference in the range of −1.5 to 1.5 samples.

The network was implemented using the Keras module of TensorFlow [32]. Keras is a high-level deep learning NN application program interface [33]. The model was created by

IEEE Access

T. H. L. Nguyen, S. Park: Intelligent Ultrasonic Flow Measurement Using Linear Array Transducer With Recurrent Neural Networks

TABLE 1. Hyperparameters of neural networks.

Hyperparameters	Fully connected NN	LSTM
Number of training data	50 000	100 000
Number of validation data	1 000	1 000
Number of test data	56	56
Input data dimensions	3300×2	33×4
Number of hidden layers	4	4
Activation function of hidden layers	ReLU	Tanh
Activation function of output layer	Linear	Linear
Optimizer	SGD	SGD
Learning rate	0.001	0.01
Loss function	MSE	MSE
Number of epochs	1000	400

sequential constructor Keras models. The stochastic gradient descent (SGD) optimizer [23] was used with a learning rate of 0.001. The mean squared error (MSE) cost function was applied to calculate the error between the target time difference after performing velocity correction and predicting the time difference (τ_{c1} and τ_{c0}) from the training and validation data. Table 1 summarizes the hyperparameters used in the fully connected NN.

3) RNN-BASED APPROACH

The LSTM is a type of RNN model used to solve the vanishing gradient problem of the conventional RNN model [23]–[28]. It is capable of learning long-term dependencies in data [23]. A typical LSTM cell comprises an input gate, an output gate, and a forget gate. The input gate controls the input flow entering the cell, whereas the output gate controls the output flow of the cell. The forget gate determines the data that should be erased for the LSTM cell. For an LSTM network with an input sequence $x = (x_1, \ldots, x_n)$ and an output sequence $y = (y_1, \ldots, y_n)$, LSTM's computation employs the following equations iteratively with t ranging from 1 to n [23]:

$$i_{(t)} = \sigma(W_{xi}^T.x_{(t)} + W_{hi}^T.h_{(t-1)} + b_i) \quad (9)$$

$$f_{(t)} = \sigma(W_{xf}^T.x_{(t)} + W_{hf}^T.h_{(t-1)} + b_f) \quad (10)$$

$$o_{(t)} = \sigma(W_{xo}^T.x_{(t)} + W_{ho}^T.h_{(t-1)} + b_o) \quad (11)$$

$$g_{(t)} = \tanh(W_{xg}^T.x_{(t)} + W_{hg}^T.h_{(t-1)} + b_g) \quad (12)$$

$$c_{(t)} = f_{(t)} \otimes c_{(t-1)} + i_{(t)} \otimes g_{(t)} \quad (13)$$

$$y_{(t)} = h_{(t)} = o_{(t)} \otimes \tanh(c_{(t)}), \quad (14)$$

where $x_{(t)}$ is the current input vector of the LSTM cell; $h_{(t-1)}$ is the previous short-term state vector; $i_{(t)}, f_{(t)}, o_{(t)},$ and $g_{(t)}$ are the input gate, forget gate, output gate, and cell state gate, respectively; $c_{(t)}$ is the long-term state vector; $h_{(t)}$ is the short-term state vector; $W_{xi}, W_{xf}, W_{xo},$ and W_{xg} are the connection weight matrices to the input vector $x_{(t)}$; $W_{hi}, W_{hf}, W_{ho},$ and W_{hg} are the connection weight matrices to the previous short-term state vector $h_{(t-1)}$; and $b_i, b_f, b_o,$ and b_g are the bias terms. In this study, we employed the RNN-based model with LSTM [24].

Fig. 5 presents the flow rate estimation process using LSTM. The dimension of the training data for the LSTM was $M \times 4$, because the data includes both flow and no-flow cases. In this model, each row of the input data was used as a sequence, such that the input data had M sequences, which

are denoted by $x_1, x_2, \ldots x_M$. The output of each LSTM cell was H (in this study, $H = 128$). Thus, the size of the output from the first LSTM layer was $M \times H$. In the second LSTM layer, a single output was selected by neglecting all outputs except for the last one (i.e., sequence to vector). Hence, the output of the second LSTM layer had a size of H. Both LSTM layers employed the hyperbolic tangent (tanh) function as the activation function. After each LSTM layer, a dropout layer was added to avoid overfitting. The dropout layer dropped the inputs and the neurons of the model, while maintaining the dimension of the output. The drop rates of the first and second dropout layers were set to 0.2 and 0.1, respectively. The final layer of the RNN-based model was the output layer for predicting the output, i.e., the time difference. Similar to the fully connected NN, the activation function of the output layer was a linear function. The target output of the RNN-based model (i.e., the time difference $\Delta\tau_c$) can be predicted without zero-flow calibration and velocity correction. Therefore, the predicted flow rate could be directly calculated from the predicted time difference $\Delta\tau_c$.

Similar to the fully connected NN model, the RNN-based model with LSTM was implemented using the Keras module of TensorFlow [32]. The optimizer was SGD with a learning rate of 0.01, and the MSE cost function was likewise applied. The hyperparameters used in the LSTM are summarized in Table 1.

D. PERFORMANCE EVALUATION

The flow rates for the 56 testing data sets were estimated to evaluate the performance of the XCorr, fully connected NN, and RNN-based model with LSTM methods. While the flow rates in the XCorr method were calculated using the algorithm, as shown in Fig. 3, the flow rates obtained using the NN approaches were predicted by the trained models of fully connected NN and RNN, as shown in Fig. 4 and 5, respectively. For each approach, linear regression using the least-squares method was employed between the reference and the estimated flow rates. Furthermore, the root mean squared error (RMSE) between the reference and estimated flow rates was computed according to the following formula:

$$RMSE = \sqrt{\frac{1}{n}\sum_{i=1}^{n}(y_i - \hat{y}_i)^2} \quad (15)$$

where y_i denotes the reference flow rate, and $\hat{y}_i$ is the flow rate estimated from our approaches. Moreover, the Bland–Altman (BA) plot [34] was constructed by plotting the differences $(y_i - \hat{y}_i)$ and averages between the reference and estimated flow rates.

To estimate the inherent error of the NN model, identical upstream and downstream data sets were used as the testing data sets for both flow and no-flow cases. Using this manipulated zero-flow case, the inherent error between zero (i.e., expected flow rate) and the predicted flow rate was calculated using the proposed NN model. All 56 experimental data sets at various flow rate levels were used to calculate the inherent error.
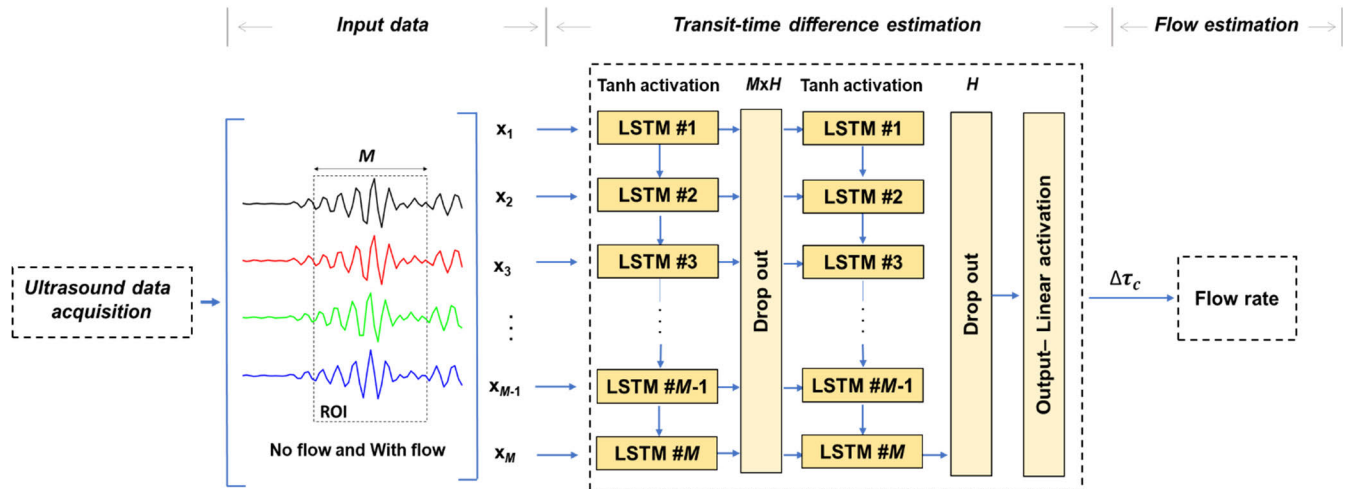
T. H. L. Nguyen, S. Park: Intelligent Ultrasonic Flow Measurement Using Linear Array Transducer With Recurrent Neural Networks

IEEE *Access*

FIGURE 5. Flow estimation block diagram for the RNN-based model with LSTM.

III. RESULTS

A. XCORR-BASED FLOW RATE ESTIMATION

Fig. 6(a) presents the estimated flow rates obtained via the XCorr method for the transit-time estimation with the reference flow rates. The regression coefficient and the intercept were 0.79 and 1.54, respectively. The RMSE between the reference and estimated flow rates of this method was 4.40. Fig. 6(b) illustrates the BA plot of the estimated and reference flow rates. The 95% confidence interval of this method ranges from –4.42 to 9.63. The BA plot indicates an overestimation of the flow rates near the 10 L/min average flow rate and an underestimation above the 15 L/min average flow rate.

B. FULLY CONNECTED NN-BASED FLOW RATE ESTIMATION

Fig. 7(a) illustrates the estimated flow rates obtained by the fully connected NN. The regression coefficient and intercept were 0.91 and 1.58, respectively. Thus, the regression coefficient was improved by 15.19% in comparison to the ultrasonic flowmeter using the XCorr method. The RMSE of this flow measurement was 4.34, which represents a 1.37% decrease relative to the XCorr method. The BA plot between the reference and estimated flow rates of the flow estimation via the fully connected NN method is shown in Fig. 7(b). The results indicate a confidence interval ranging from –8.46 to 8.71. The confidence interval of the flowmeter using the fully connected NN (i.e., 17.17) was 22.21% higher than the flow estimation utilizing the XCorr method (i.e., 14.05). The underestimation at higher flow rates was improved, as indicated by a 9.55% reduction in the confidence limit of the fully connected NN (8.71) relative to that of the XCorr method (9.63). Overall, the flow rate estimation using the fully connected NN exhibited higher variations than the XCorr method. Although various hyperparameters were tested, the performance of the fully connected NN was not sufficient to replace the XCorr method for the estimation of flow rates.

C. RNN-BASED FLOW RATE ESTIMATION

Fig. 8 presents the training and validation losses of the RNN-based model during the 400 training epochs. Overall, the training and validation loss decreased during training. The loss decreased significantly from epoch 100 to 150. After 400 epochs, the training and validation losses were 0.0022 and 0.0019, respectively. The validation loss of the RNN-based model was lower than that of the fully connected NN (i.e., 0.0019 and 0.0024, respectively).

Fig. 9 shows the flow rates predicted using the proposed intelligent ultrasonic flowmeter employing the RNN-based model with LSTM. The linear regression in Fig. 9(a) exhibited a higher regression coefficient of 0.94 (increments of 3.30% and 18.99% compared to the fully connected NN and XCorr, respectively) and a lower intercept of 0.84 (reduction of 46.84% and 45.45% compared to the fully connected NN and XCorr, respectively). Furthermore, the RMSE (2.93) was lower than that of the fully connected NN (32.55% reduction) and XCorr methods (33.48% reduction). Based on the BA plot (Fig. 9(b)), the RNN-based approach had a narrower confidence interval (–5.38 to 6.11), which was 18.22% and 33.08% lower than those of the XCorr and fully connected NN methods, respectively. Nevertheless, there was an underestimation near the flow rate of 50 L/min; however, it was significantly subsided compared to the BA plot of the XCorr method. The linear regression, RMSE, and BA plots indicate significant improvements in the ultrasound flow estimation of the proposed RNN-based model with LSTM. Thus, it was demonstrated that the intelligent ultrasonic flowmeter using the LSTM yields higher accuracy and precision than the XCorr and fully connected NN methods.

IV. DISCUSSION

The current study demonstrates the feasibility of intelligent transit-time ultrasonic flow measurement using an RNN-based approach. Table 2 summarizes the performance of the ultrasonic flowmeter obtained via different approaches,
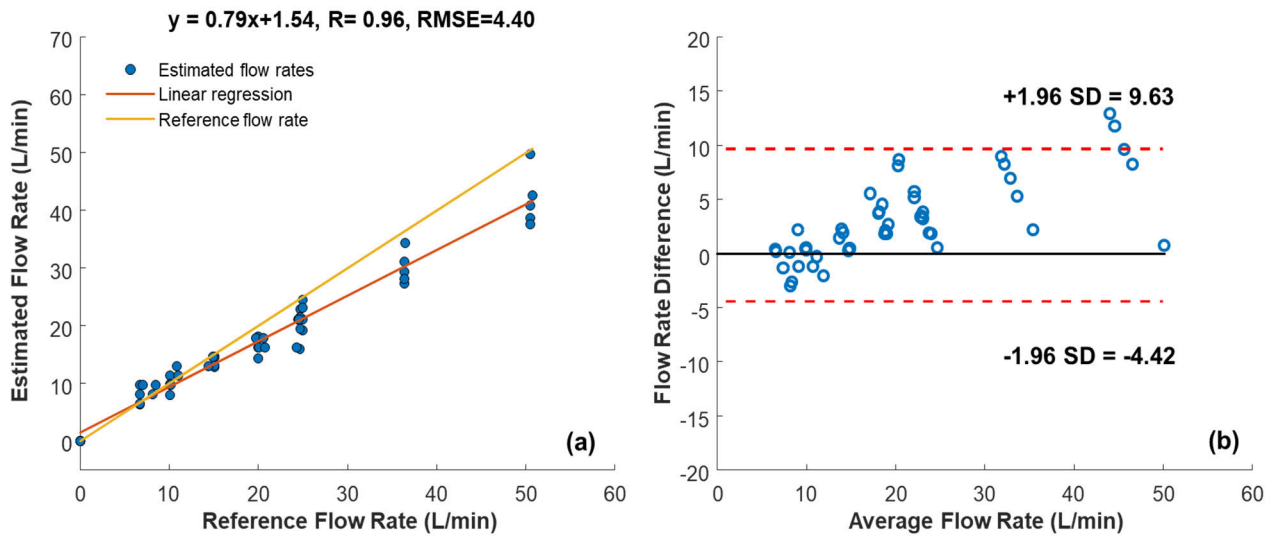
IEEE *Access*

T. H. L. Nguyen, S. Park: Intelligent Ultrasonic Flow Measurement Using Linear Array Transducer With Recurrent Neural Networks

FIGURE 6. Flow rates estimated using the XCorr method. (a) Linear regression; (b) Bland–Altman plot.
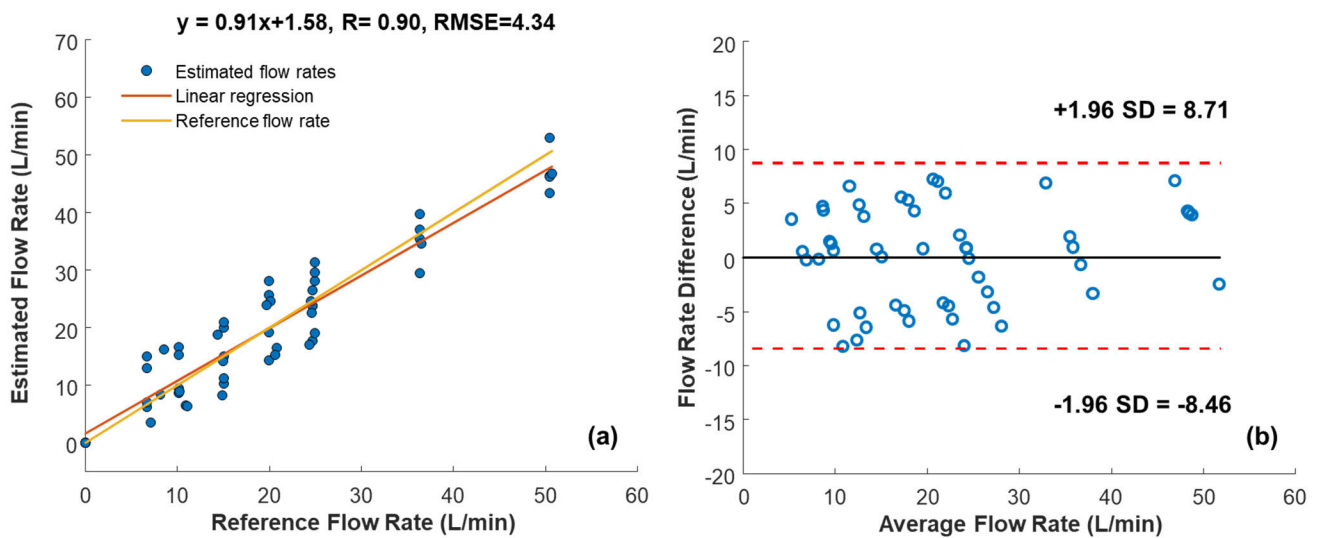

FIGURE 7. Estimated flow rates using the fully connected NN. (a) Linear Regression; (b) Bland-Altman plot.

including the XCorr, fully connected NN, and RNN-based LSTM methods. The proposed RNN-based model with LSTM (Fig. 5) improves the performance of the transit-time difference estimation and is also capable of replacing the entire process of flow rate estimation, including interpolation, velocity correction, and zero-flow calibration. The required input for the RNN-based model is the sequence of signals from both cases with and without a flow. As the transit-time differences after zero-flow compensation and velocity correction were used as the target output of the RNN-based model during training, the output of the RNN-based model can be used to directly calculate the flow rate. While the RNN-based model was implemented without interpolation of the input data, the fully connected NN required 100 times interpolation

for the input data to implement the deeper layer NN. Although not included in this paper, the performance of the fully connected NN model did not yield any improvement, even with twice the training data, as compared to other approaches. The possibility to improve the fully connected NN by using different layers or hyperparameters still exists; however, the RNN-based model is more suitable for the time series or sequence data used in this study. Furthermore, the LSTM can utilize long-term memory to improve the prediction accuracy of the transit-time difference.

Because the low sampling rate of the flowmeter induces errors in transit-time flow estimation, a sampling frequency at least ten times the transducer transmission frequency is required to achieve high accuracy and precision suitable for
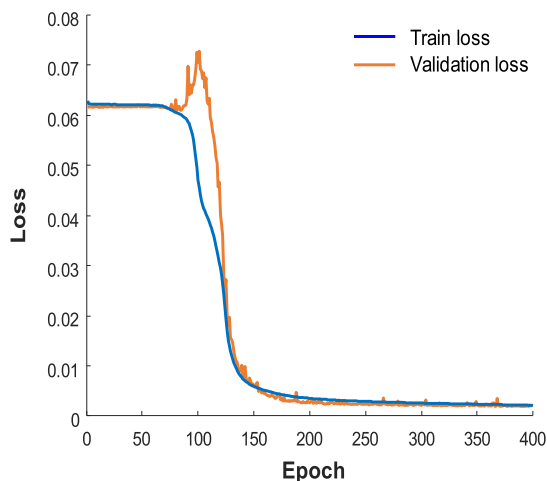
T. H. L. Nguyen, S. Park: Intelligent Ultrasonic Flow Measurement Using Linear Array Transducer With Recurrent Neural Networks

IEEE *Access*

FIGURE 8. Loss curves of the RNN-based model.

TABLE 2. Performance evaluation of ultrasonic flowmeter.

Parameters	XCorr	Fully connected NN	LSTM
Regression coefficient	0.79	0.91	0.94
Intercept	1.54	1.58	0.84
R	0.96	0.90	0.95
RMSE	4.40	4.34	2.93
Confidence interval	14.05	17.17	11.49

industrial applications [11]. In this study, the sampling rate of the ultrasonic flowmeter was four times the transducer transmission frequency. While the XCorr method yielded an accuracy of 79% and an RMSE of 4.40 (Fig. 6), the RNN-based approach achieved an accuracy of 94% with an RMSE of 2.93 (Fig. 9). Thus, the proposed RNN-based ultrasonic flow measurement was capable of reducing the performance degradation caused by the sampling rate limitation. From the BA plots of the XCorr, fully connected NN,

and RNN-based approaches, underestimation (i.e., above zero flow rate difference) was observed at high flow rates (> 15 L/min for XCorr and > 40 L/min for both the fully connected NN and the RNN-based approach). When the flow rate increases, bubbles are generated in the fluid, which compromises the quality of the ultrasonic signal [9]. Although bubble generation in the liquid flow was unavoidable, we could observe that the overestimation was significantly reduced in the RNN-based approach. In addition to the RMSE error, the relative error between the estimated and the reference flow rates can also be calculated. The mean of the relative errors for XCorr, fully connected NN, and RNN-based methods were 12.99%, 22.24%, and 10.93%, respectively. The relative error of the RNN-based approach was reduced by 15.86%, as compared to that of the XCorr method. The overall relative error is substantially high, as the current approach employs non-invasive measurement with a single path in a minimized pipe system (i.e., narrow and short pipe lengths). Although this study compared the performance of different approaches, future research should focus on further improvements involving the multi-path approach.

Fig. 10(a) presents the distribution of the target flow rates of 100,000 training data sets used for the proposed RNN-based model, indicating that the target flow rates from 0 L/min to 70 L/min were uniformly distributed with frequencies of 6000–7000. Fig. 10(b) presents the inherent error of the RNN-based model. Overall, the inherent error of the proposed RNN-based model is overestimated. The error between the estimated flow rates and the zero-flow rates varied from –6.40 L/min to 2.13 L/min. The inherent noise of the proposed RNN-based model (Fig. 10(b)) was mostly overestimated. As the target flow rates are positive numbers, as shown in Fig. 10(a), the overestimation of the manipulated zero-flow case was predictable. Although this manipulated case does not occur during the actual flow measurement experiment, this result indicates the limitation of the RNN-based model
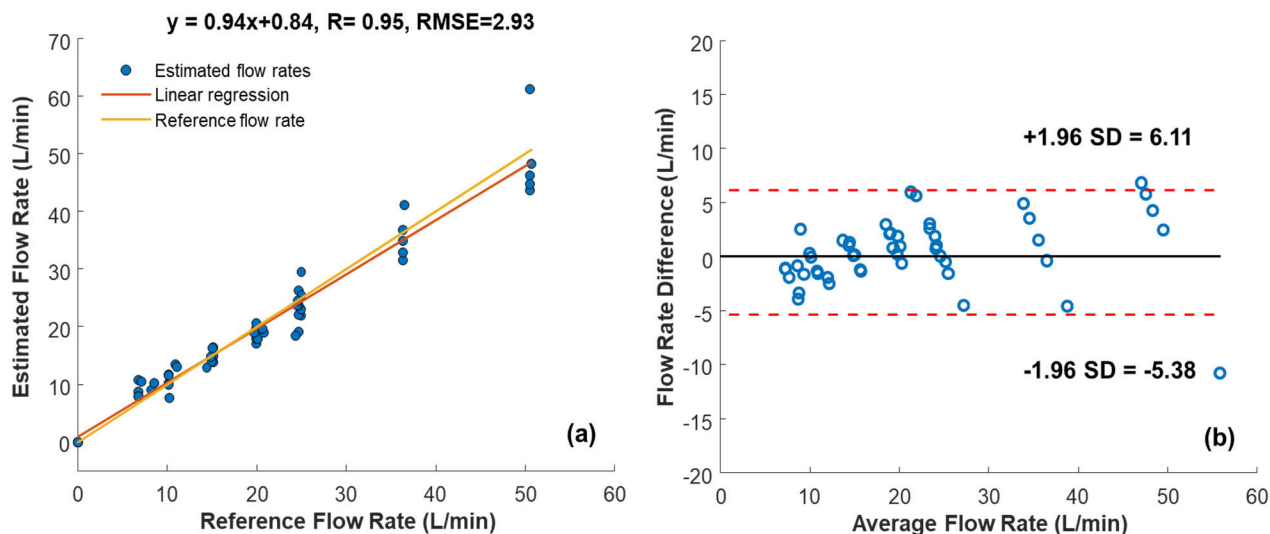

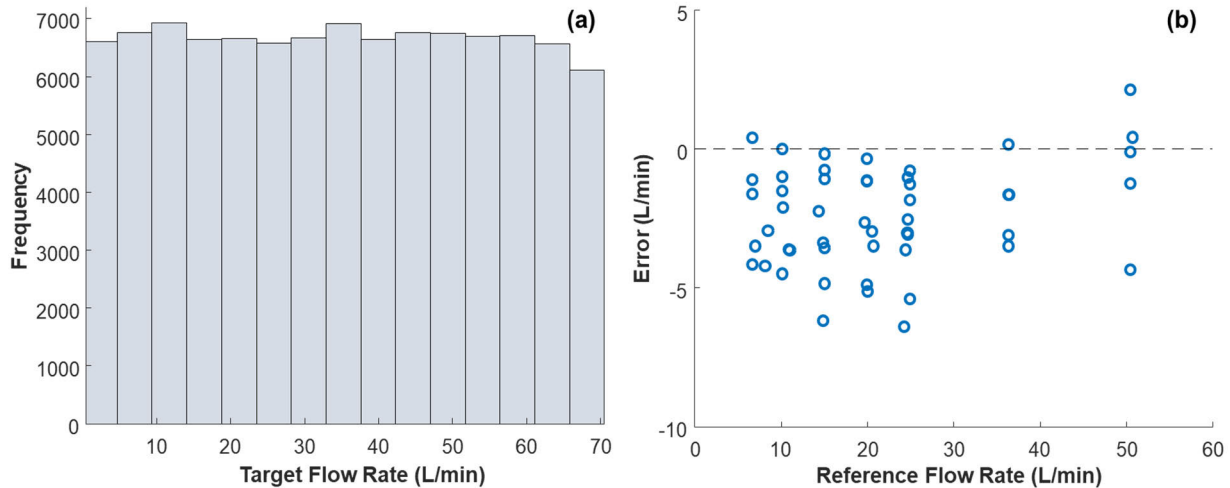**FIGURE 9.** Estimated flow rates using LSTM. (a) Linear Regression; (b) Bland–Altman plot.

FIGURE 10. (a) Distribution of target flow rates of training data for LSTM. (b) Inherent error of the LSTM.

when absolutely no flow is expected. It should be noted that zero-flow data are required as the input for training the RNN-based model. These zero-flow data are simulated to train the model. Subsequently, for flow measurements, actual zero-flow data can be acquired when the flowmeter is first installed or when the physical conditions of the pipe are altered. Once the network had been trained, the stored zero-flow data can be utilized for flow measurements.

Training data are essential to realize an intelligent ultrasound flowmeter based on deep learning, because their quantity and quality determine the performance of the NN. In this study, the training data were generated through a simulation with a known transit-time difference using experimental data. The results in this study demonstrated that this simulated training data helped improve the training process and reduced the error in prediction. Although we only considered the average velocity through the ultrasonic travel path in the pipe, training data considering the velocity profile in the pipe can also be utilized for further improvements in flow estimations [14], [15]. Using a single CPU (Intel i7-8700) with 16 GB memory, the computational time required for network training was 2.5 h and 27 h for the fully connected NN and RNN-based model with LSTM, respectively. Once the network training is completed, the computed network requires only a few seconds to run. Thus, the trained network can be embedded in the device for flow measurements.

From an industrial perspective, the proposed approach could potentially be applied to the water pipes in pump stations, where accurate flow measurements can help control and manage the pump, thereby improving the energy efficiency of buildings [5]. In industries, flow measurement is applied to different pipe systems under various conditions. Therefore, ultrasonic flowmeters must be adaptable to various pipe specifications. The intelligent ultrasonic flowmeter exploits the flexibility of the NN-based approach. The RNN-based approach can be easily trained for various situations, provided the pipe specifications and experimental

data are given. Furthermore, our approach can be applied for various fluids, as long as the particles in the fluid are smaller than the wavelength of the ultrasound wave ($< 300 \ \mu$m in this study). Moreover, the wavelength can be controlled by varying the frequency of the ultrasound wave. Thus, the proposed RNN-based flow estimation model shows potential for industrial applications. In this study, we presented the feasibility of using the RNN-based model for the entire process of flow estimation utilizing one-dimensional data. As two-dimensional data from the array transducer can also be utilized effectively, our future research will involve designing a NN model employing two-dimensional data, such as the convolutional LSTM NN [35], [36], for further improvements in intelligent ultrasonic flow estimation.

V. CONCLUSION
In order to improve the transit-time difference estimation of ultrasonic flowmeter, this study demonstrates intelligent ultrasonic fluid flow measurements by employing an RNN-based model with LSTM. The RNN-based approach includes the entire process of ultrasonic flow estimation in a pipe system, which are interpolation, transit-time difference estimation, zero-flow calibration, and velocity correction. The proposed intelligent ultrasonic flowmeter yields superior performance in the experimental study, with high accuracy and low errors compared with the Xcorr and fully connected NN approaches, thereby demonstrating its suitability for industrial applications.

REFERENCES
[1] R. W. Miller, *Flow Measurement Engineering Handbook*. Pittsburgh, PA, USA: Instrument Society of America, 1983.
[2] L. C. Lynnworth and Y. Liu, "Ultrasonic flowmeters: Half-century progress report, 1955-2005," *Ultrasonics*, vol. 44, pp. 1371–1378, 2006, doi: 10.1016/j.ultras.2006.05.046.

T. H. L. Nguyen, S. Park: Intelligent Ultrasonic Flow Measurement Using Linear Array Transducer With Recurrent Neural Networks

IEEE Access

[3] M. L. Sanderson and H. Yeung, "Guidelines for the use of ultrasonic non-invasive metering techniques," *Flow Meas. Instrum.*, vol. 13, no. 4, pp. 125–142, Aug. 2002, doi: 10.1016/S0955-5986(02)00043-2.

[4] E. Mandard, D. Kouame, R. Battault, J.-P. Remenieras, and F. Patat, "Methodology for developing a high-precision ultrasound flow meter and fluid velocity profile reconstruction," *IEEE Trans. Ultrason., Ferroelectr., Freq. Control*, vol. 55, no. 1, pp. 161–172, 2008, doi: 10.1109/TUFFC.2008.625.

[5] M. A. Moreno, P. A. Carrión, P. Planells, J. F. Ortega, and J. M. Tarjuelo, "Measurement and improvement of the energy efficiency at pumping stations," *Biosystems Eng.*, vol. 98, no. 4, pp. 479–486, Dec. 2007, doi: 10.1016/j.biosystemseng.2007.09.005.

[6] J. Hemp, "Theory of transit time ultrasonic flowmeters," *J. Sound Vib.*, vol. 84, no. 1, pp. 133–147, Sep. 1982, doi: 10.1016/0022-460X(82)90437-0.

[7] G. Rajita and N. Mandal, "Review on transit time ultrasonic flowmeter," in *Proc. 2nd Int. Conf. Control, Instrum., Energy Commun. (CIEC)*, Jan. 2016, pp. 88–92, doi: 10.1109/CIEC.2016.7513740.

[8] J. Han, H. Liu, Y. Zhou, R. Zhang, and C. Li, "Studies on the transducers of clamp-on transit-time ultrasonic flow meter," in *Proc. 4th IEEE Int. Conf. Inf. Sci. Technol.*, Apr. 2014, pp. 180–183, doi: 10.1109/ICIST.2014.6920360.

[9] T. H. L. Nguyen and S. Park, "Multi-angle liquid flow measurement using ultrasonic linear array transducer," *Sensors*, vol. 20, no. 2, p. 388, Jan. 2020, doi: 10.3390/s20020388.

[10] A. Hamouda, O. Manck, M. Hafiane, and N.-E. Bouguechal, "An enhanced technique for ultrasonic flow metering featuring very low jitter and offset," *Sensors*, vol. 16, no. 7, p. 1008, Jun. 2016, doi: 10.3390/s16071008.

[11] T. Moazzeni, J. Ma, Y. Jiang, and N. Li, "Flow rate measurement in a high-temperature, radioactive, and corrosive environment," *IEEE Trans. Instrum. Meas.*, vol. 60, no. 6, pp. 2062–2069, Jun. 2011, doi: 10.1109/TIM.2011.2115370.

[12] T. T. Yeh, P. I. Espina, and S. A. Osella, "An intelligent ultrasonic flowmeter for improved flow measurement and flow calibration facility," in *Proc. 18th IEEE Instrum. Meas. Technol. Conf. Rediscovering Meas. Age Inform. (IMTC)*, vol. 3, May 2001, pp. 1741–1746, doi: 10.1109/IMTC.2001.929499.

[13] L. Qin, L. Hu, K. Mao, W. Chen, and X. Fu, "Flowrate determination for arbitrary multipath arrangement based on generalized inverse of matrix," *IEEE Sensors J.*, vol. 17, no. 12, pp. 3625–3634, Jun. 2017.

[14] E. Luntta and J. Halttunen, "Neural network approach to ultrasonic flow measurements," *Flow Meas. Instrum.*, vol. 10, no. 1, pp. 35–43, Mar. 1999, doi: 10.1016/S0955-5986(98)00035-1.

[15] H. Zhao, L. Peng, T. Takahashi, T. Hayashi, K. Shimizu, and T. Yamamoto, "ANN based data integration for multi-path ultrasonic flowmeter," *IEEE Sensors J.*, vol. 14, no. 2, pp. 362–370, Feb. 2014.

[16] L. Qin, L. Hu, K. Mao, W. Chen, and X. Fu, "Application of extreme learning machine to gas flow measurement with multipath acoustic transducers," *Flow Meas. Instrum.*, vol. 49, pp. 31–39, Jun. 2016.

[17] L. Hu, L. Qin, K. Mao, W. Chen, and X. Fu, "Optimization of neural network by genetic algorithm for flowrate determination in multipath ultrasonic gas flowmeter," *IEEE Sensors J.*, vol. 16, no. 5, pp. 1158–1167, Mar. 2016.

[18] C. M. Bishop, "Neural networks and their applications," *Rev. Sci. Instrum.*, vol. 65, no. 6, pp. 1803–1832, 1994.

[19] Y. LeCun, Y. Bengio, and G. Hinton, "Deep learning," *Nature*, vol. 521, pp. 436–444, May 2015.

[20] J. Schmidhuber, "Deep learning in neural networks: An overview," *Neural Netw.*, vol. 61, pp. 85–117, Jan. 2015, doi: 10.1016/j.neunet.2014.09.003.

[21] M. Z. Alom, T. M. Taha, C. Yakopcic, S. Westberg, P. Sidike, M. S. Nasrin, M. Hasan, B. C. Van Essen, A. A. S. Awwal, and V. K. Asari, "A state-of-the-art survey on deep learning theory and architectures," *Electronics*, vol. 8, no. 3, p. 292, Mar. 2019, doi: 10.3390/electronics8030292.

[22] M. Y. Rafiq, G. Bugmann, and D. J. Easterbrook, "Neural network design for engineering applications," *Comput. Struct.*, vol. 79, no. 17, pp. 1541–1552, 2001, doi: 10.1016/S0045-7949(01)00039-6.

[23] A. Géron, *Hands-On Machine Learning with Scikit-Learn, Keras, and TensorFlow: Concepts, Tools, and Techniques to Build Intelligent Systems.* Newton, MA, USA: O'Reilly Media, 2019.

[24] S. Hochreiter and J. J. Schmidhuber, "Long short-term memory," *Neural Comput.*, vol. 9, no. 8, pp. 1735–1780, 1997, doi: 10.1162/neco.1997.9.8.1735.

[25] H. Sak, A. W. Senior, and F. Beaufays, "Long short-term memory recurrent neural network architectures for large scale acoustic modeling," in *Proc. Interspeech*, 2014, pp. 1–5.

[26] K. Greff, R. K. Srivastava, J. Koutnik, B. R. Steunebrink, and J. Schmidhuber, "LSTM: A search space odyssey," *IEEE Trans. Neural Netw. Learn. Syst.*, vol. 28, no. 10, pp. 2222–2232, Oct. 2017.

[27] X. Du, H. Zhang, H. V. Nguyen, and Z. Han, "Stacked LSTM deep learning model for traffic prediction in vehicle-to-vehicle communication," in *Proc. IEEE 86th Veh. Technol. Conf. (VTC-Fall)*, Sep. 2017, pp. 1–5, doi: 10.1109/VTCFall.2017.8288312.

[28] P. J. Jino, J. John, and K. Balakrishnan, "Offline handwritten malayalam character recognition using stacked LSTM," in *Proc. Int. Conf. Intell. Comput., Instrum. Control Technol. (ICICICT)*, Jul. 2017, pp. 1587–1590, doi: 10.1109/ICICICT1.2017.8342807.

[29] R. Cabot, "A note on the application of the Hilbert transform to time delay estimation," *IEEE Trans. Acoust., Speech, Signal Process.*, vol. 29, no. 3, pp. 607–609, Jun. 1981.

[30] M. A. Lubinski, S. Y. Emelianov, and M. O'Donnell, "Speckle tracking methods for ultrasonic elasticity imaging using short-time correlation," *IEEE Trans. Ultrason., Ferroelectr., Freq. Control*, vol. 46, no. 1, pp. 82–96, Jan. 1999, doi: 10.1109/58.741427.

[31] H. Zhang, C. Guo, and J. Lin, "Effects of velocity profiles on measuring accuracy of transit-time ultrasonic flowmeter," *Appl. Sci.*, vol. 9, no. 8, p. 1648, Apr. 2019, doi: 10.3390/app9081648.

[32] M. Abadi, P. Barham, J. Chen, Z. Chen, A. Davis, J. Dean, M. Devin, S. Ghemawat, G. Irving, M. Isard, and M. Kudlur, "Tensorflow: A system for large-scale machine learning," in *Proc. Symp. Operating Syst. Des. Implement.*, 2016, pp. 265–283.

[33] F. Chollet. (2015). *Keras.* [Online]. Available: https://keras.io

[34] D. Giavarina, "Understanding bland altman analysis," *Biochemia Medica*, vol. 25, no. 2, pp. 141–151, 2015, doi: 10.11613/BM.2015.015.

[35] H. Liu, X. Mi, and Y. Li, "Smart deep learning based wind speed prediction model using wavelet packet decomposition, convolutional neural network and convolutional long short term memory network," *Energy Convers. Manage.*, vol. 166, pp. 120–131, Jun. 2018, doi: 10.1016/j.enconman.2018.04.021.

[36] D. Balderas, P. Ponce, and A. Molina, "Convolutional long short term memory deep neural networks for image sequence prediction," *Expert Syst. Appl.*, vol. 122, pp. 152–162, May 2019, doi: 10.1016/j.eswa.2018.12.055.

THI HUONG LY NGUYEN received the B.S. degree in energy from the University of Science and Technology of Hanoi, Hanoi, Vietnam, in 2017. She is currently pursuing the M.S. degree with the School of Electrical and Electronics Engineering, Chung-Ang University, Seoul, South Korea. Her research interests include signal processing, ultrasonic flow estimation, and deep learning.

SUHYUN PARK received the B.S. and M.S. degrees in electronics engineering from Ewha Womans University, Seoul, South Korea, in 1999 and 2001, respectively, and the Ph.D. degree in biomedical engineering from The University of Texas at Austin, Austin, TX, USA, in 2008.

From 2003 to 2008, she worked as a Research Assistant with the Ultrasound and Therapeutic Research Laboratory. In 2008, she joined the Imaging Technology Group, GE Global Research, Niskayuna, NY, USA, and worked as a Scientist and a Systems Engineer on advanced ultrasound imaging applications. In 2012, she joined the Samsung Advanced Institute of Technology, Suwon, Gyeonggi, South Korea and worked as a Research Staff Member. Since 2017, she has been a Professor with the School of Electrical and Electronics Engineering, Chung-Ang University, Seoul. She has authored more than 60 articles and patented more than ten inventions. Her research interests include ultrasound imaging, ultrasonic flow estimation, and research on biosignal analysis.

• • •